ResearchGate

See discussions, stats, and author profiles for this publication at: http://www.researchgate.net/publication/221893348

Precise measurement of renal filtration and vascular parameters using a two-compartment model for dynamic contrast-enhanced MRI of the kidney gives realistic normal values.

ARTICLE *in* EUROPEAN RADIOLOGY · MARCH 2012

Impact Factor: 4.34 · DOI: 10.1007/s00330-012-2382-9 · Source: PubMed

CITATIONS
7

DOWNLOADS
136

VIEWS
186

5 AUTHORS, INCLUDING:

Paul Stephen Tofts
University of Sussex
238 PUBLICATIONS **14,152** CITATIONS

SEE PROFILE

Marica Cutajar
University College London
15 PUBLICATIONS **197** CITATIONS

SEE PROFILE

Iosif A Mendichovszky
University of Cambridge
12 PUBLICATIONS **271** CITATIONS

SEE PROFILE

Available from: Marica Cutajar
Retrieved on: 14 July 2015

Eur Radiol (2012) 22:1320–1330
DOI 10.1007/s00330-012-2382-9

MAGNETIC RESONANCE

Precise measurement of renal filtration and vascular parameters using a two-compartment model for dynamic contrast-enhanced MRI of the kidney gives realistic normal values

Paul S. Tofts · Marica Cutajar · Iosif A. Mendichovszky · A. Michael Peters · Isky Gordon

Received: 29 August 2011 / Revised: 25 November 2011 / Accepted: 4 December 2011 / Published online: 14 March 2012
© European Society of Radiology 2012

Abstract
Objective To model the uptake phase of T_1-weighted DCE-MRI data in normal kidneys and to demonstrate that the fitted physiological parameters correlate with published normal values.
Methods The model incorporates delay and broadening of the arterial vascular peak as it appears in the capillary bed, two distinct compartments for renal intravascular and extravascular Gd tracer, and uses a small-vessel haematocrit value of 24%. Four physiological parameters can be estimated: regional filtration K^{trans} (ml min^{-1} [ml tissue]$^{-1}$), perfusion F (ml min^{-1} [100 ml tissue]$^{-1}$), blood volume v_b (%) and mean residence time MRT (s). From these are found the filtration fraction (*FF*; %) and total GFR (ml min^{-1}). Fifteen healthy volunteers were imaged twice using oblique coronal slices every 2.5 s to determine the reproducibility.
Results Using parenchymal ROIs, group mean values for renal biomarkers all agreed with published values: K^{trans}: 0.25; F: 219; v_b: 34; MRT: 5.5; *FF*: 15; GFR: 115. Nominally cortical ROIs consistently underestimated total filtration (by ~50%). Reproducibility was 7–18%. Sensitivity analysis showed that these fitted parameters are most vulnerable to errors in the fixed parameters kidney T_1, flip angle, haematocrit and relaxivity.
Conclusions These renal biomarkers can potentially measure renal physiology in diagnosis and treatment.
Key Points
- *Dynamic contrast-enhanced magnetic resonance imaging can measure renal function.*
- *Filtration and perfusion values in healthy volunteers agree with published normal values.*
- *Precision measured in healthy volunteers is between 7 and 15%.*

Keywords DCE-MRI · Kidney · GFR · Quantification · Modeling

Electronic supplementary material The online version of this article (doi:10.1007/s00330-012-2382-9) contains supplementary material, which is available to authorized users.

P. S. Tofts · M. Cutajar · A. M. Peters
Brighton and Sussex Medical School,
Falmer, Sussex BN1 9PX, UK

P. S. Tofts
UCL Institute of Neurology,
London WC1N 3BG, UK

M. Cutajar · I. Gordon
UCL Institute of Child Health,
London WC1N 3JH, UK

I. A. Mendichovszky
Imaging Science and Biomedical Engineering,
University of Manchester,
Manchester M20 3LJ, UK

P. S. Tofts (✉)
48 Rugby Road,
Brighton BN1 6EB, UK
e-mail: bsms@paul-tofts.org.uk

Introduction

Dynamic imaging of renal uptake of a contrast agent is an established way of assessing renal physiology using nuclear medicine, dynamic computed tomography and magnetic resonance imaging (MRI), and estimation of quantitative parameters is possible [1–8]. Several reviews are available [9–11].

Dynamic contrast-enhanced (DCE) MRI of the kidneys is now clinically feasible with the advent of fast sequences.

This paper builds on the compartmental modelling approach that has been so successful in characterising capillary leakage in tumours [12, 13], with the addition of a delay and broadening of the arterial vascular peak as is observed in the kidney. This is most likely caused by a small delay along the renal artery and a non-zero residence time in the renal capillary bed. The renal model, applicable to cortical and parenchymal ROIs, captures the essential features of the dynamic data, yet remains simple.

The published modelling work in normal subjects generally shows little systematic effort to reconcile the measurements with published values from other (non-MRI) methods, and there are few systematic measurements of precision (repeatability). Very often DCE images are just reported visually (i.e. qualitatively). In this quantitative study, testing the new model using data from healthy volunteers shows that key renal physiological parameters related to filtration and perfusion are estimated with good reproducibility and give measurements close to published normal values. Preliminary versions of this work have been presented orally [14–16]. This paper should be read with the Electronic Supplementary Material (ESM).

Materials and methods

Pharmacokinetic and MRI model

The model consists of two parts (full mathematical details are given in the Appendix). The pharmacokinetic part (see Fig. 1 and Eqs. 1–5 below) is applicable to the cortex and parenchyma. It describes the intra-renal concentrations of intravascular (IV; largely glomerular) and extravascular (EV; mostly tubular) Gd contrast agent (also called tracer) in renal tissue (Fig. 1). The arterial vascular peak is delayed and broadened (dispersed) before arrival at the IV compartment (the delay is apparent in the data, see Fig. 3a below). This process is described by a vascular impulse response function (VIRF); thus, the IV plasma concentration in the kidney is the convolution of the arterial plasma concentration with the VIRF (Eq. 1 below). The VIRF is the response in the renal vasculature to a very short pulse (in fact a mathematical delta function) of Gd in the aorta (see Fig. 6 below). From the VIRF renal perfusion F (ml blood min^{-1} (100 ml tissue)$^{-1}$) was estimated. Uptake or flux from the IV to the EV compartment (by the process of filtration, whereby Gd is removed from capillaries) is $F_1 = K^{trans} C_p^{kid}(t)$ per unit volume of tissue, where K^{trans} is the regional filtration (GFR per unit volume of kidney; formally the volume transfer constant [12] from plasma), $C_p^{kid}(t)$ is the time-varying tracer plasma concentration in the IV compartment, and F_1 has units of mmol min^{-1} (ml tissue)$^{-1}$. This transportation of Gd into the ROI by vascular means is appropriate in a cortical or parenchymal ROI, but not in a medullary ROI.

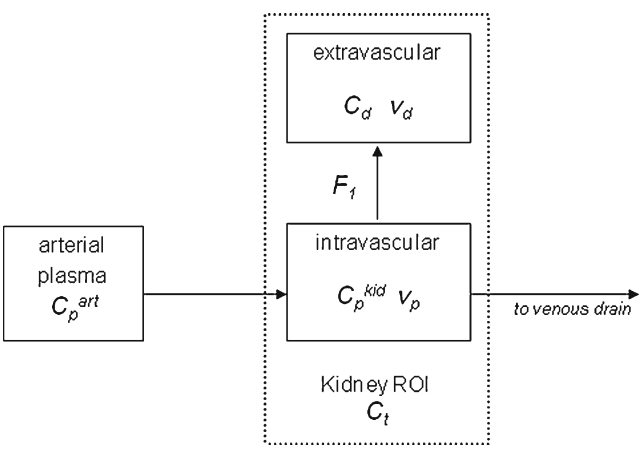

Fig. 1 Two-compartment model for renal filtration. The intravascular (IV) compartment is primarily glomerular; the extravascular (EV) compartment is primarily tubular. The dotted box represents an ROI or pixel in the kidney. This model is used soon after Gd bolus arrival, before there is time for efflux from the EV compartment

It is known [4, 17] that no filtered tracer leaves the kidney for a certain time after arrival in the blood capillaries (if a parenchymal region is used, this time is usually about 90 s); the model is used to analyse data over this relatively short time period, and therefore it can be assumed that there is no efflux from the EV compartment.

The MRI part of the model (Eqs. 6–9) defines how Gd concentration enhances the MRI signal. It relies on knowledge of several fixed parameter values (see Table 1 below): T_1 of blood and kidney, Gd relaxivity, haematocrit, and the imaging parameters TR and flip angle FA.

In the fitting procedure, the model is adjusted by varying the free parameters in the model until the difference between

Table 1 Filtration values and fit residuals from the uptake phase of repeated imaging of 15 healthy volunteers

ROI	VIRF	K^{trans} (min^{-1})			RMS residual
		Mean	SD[a]	ISD[b]	(Mean; %)
Cortical	Delayed exponential	0.29	0.058	0.046	3.9
	Gaussian	0.30	0.060	0.046	4.8
Parenchymal	Delayed exponential	0.25	0.058	0.043	4.0
	Gaussian	0.25	0.059	0.043	4.5

VIRF = vascular impulse response function, ISD = instrumental standard deviation, RMS = root-mean-square

[a] Group SD

[b] Instrumental SD (from repeated imaging)

the model and the measured signal data is minimised. The free parameters are the filtration K^{trans}, the blood volume v_b and the VIRF parameters (one for broadening, and if necessary a second parameter to describe delay). Thus the instant exponential VIRF was defined by only one free parameter, whilst the delayed exponential and Gaussian VIRFs required two free parameters (see Appendix). For each fit the RMS (root-mean-square) residual (i.e. difference between a data point and the model value) was found. The local filtration fraction is the ratio of regional filtration to regional renal plasma flow, and was calculated using Eq. 10.

MRI acquisition and analysis

Fifteen healthy volunteers were imaged twice (about 13 days apart) at 1.5 T with a temporal resolution of 2.5 s. A half-dose of Gd-DPTA was used. No T_1 values were measured. Image datasets were registered to remove in-plane movement [18]. Regions of interest (ROIs) were placed over the aorta and kidney. A parenchymal ROI was defined semi-automatically on the perfusion image as proposed by Peters et al. [19]. An ROI of the whole cortex was drawn manually (Fig. 2). Full details of MRI acquisition and ROI generation are given in the ESM.

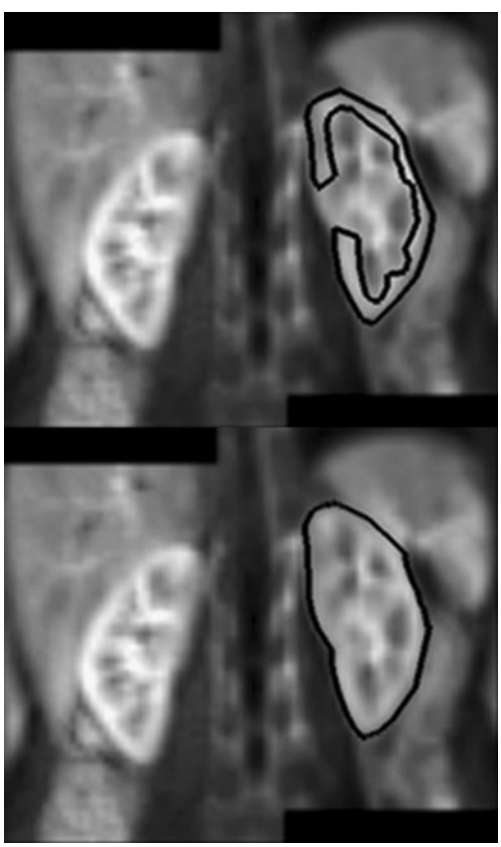

Fig. 2 Cortical and parenchymal ROIs

In the model analysis, two phases (i.e. time periods) of data were fitted: (1) the perfusion phase (up to the kidney signal minimum after the first bolus passage) when Gd is largely IV, and (2) the uptake (filtration) phase (up to 90 s after bolus arrival, before any Gd has left the parenchymal ROI). Renal filtration and vascular parameters (including local filtration, filtration fraction, perfusion, blood volume and mean residence time) were estimated. We hypothesised that vascular parameters might be better estimated from perfusion phase data than from uptake phase data; fits were compared on the basis of reproducibility and residuals.

Three plausible VIRFs (instant exponential, delayed exponential and Gaussian) were compared in cortical and parenchymal ROIs on the basis of the quality of the model fit and the reproducibility of perfusion estimates. The values of the seven fixed tissue parameters (see Table 5) were initially set at: Hct^{large}=Hct^{small}=41% [20]; $r_1^{blood} = r_1^{d} = r_1^{iv} = 4.5\mathrm{s}^{-1}\mathrm{mM}^{-1}$ (the in vitro value [21]); $T_{10}^{blood} = 1.4s$ [22]; $T_{10}^{kidney} = 1.2\mathrm{s}$ (average of cortical and medullary values [23]).

Instrumental SD (ISD) For each kidney, the differences in repeated measures of model parameters were calculated, to give the standard deviation in a single measurement, using the method of Bland and Altman [24]. In this approach, the differences between repeated measurements in the same subject are found; the standard deviation of these differences are calculated and then divided by 1.4 to find the standard deviation in a single measurement [25].

Total filtration The filtration parameter found by the model (GFR per unit volume of tissue, or K^{trans}) is an intensive quantity (thus density and temperature are intensive quantities as they do not automatically increase with size, as mass does). A relationship can be established between K^{trans} and GFR, which is the quantity used clinically. From the mean K^{trans} in a ROI, the total filtration in that ROI can be found (GFR_ROI = K^{trans} × ROI volume). As increasingly large ROIs are used, we expect to see a plateau in GFR_ROI, as all of the functioning kidney in that slice is included. ROIs of increasing size were created manually, from a small piece of cortex up to ROIs that were larger than ('over included') all of the parenchyma in a slice. (Here 'over-inclusion' means that all the partial-volume pixels that could possibly be part of the parenchyma were included.) This object strength approach overcomes partial volume effects and the difficulty of drawing precise ROIs, and has been used to characterise objects with indistinct borders [26]. Eight kidney datasets were analysed (2 subjects, each with repeated imaging).

Model sensitivity analysis The vulnerability of the various tissue parameter estimates ($K_{v_b}^{trans}$ etc., see Table 5 below) to

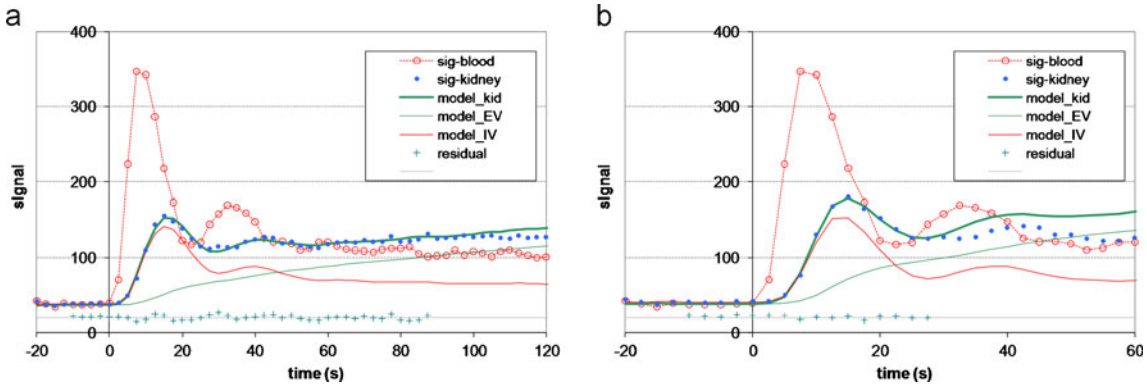

Fig. 3 Example fits of model to data from a single healthy kidney, showing two phases of data, with delayed Gaussian vascular impulse response function (VIRF). **a** Parenchymal ROI, uptake phase; **b** cortical ROI, perfusion phase. Residuals are shown for fitting period only (vertically offset in the plot, for clarity). Note evidence of efflux after the end of the fitting period (data dip below model). Separate IV and EV contributions to the model are shown

error in the fixed parameters (r_1, T_{10} etc.) was found by calculating the error propagation ratio (EPR) [27]. In this sensitivity analysis, the model is used to determine by what percentage a tissue parameter estimate will change as a result of a 1% error in a fixed parameter. For example a +1% error in T_{10}^{kid} will cause an approximately -1% error in K^{trans}; thus the EPR from T_{10}^{kid} to K^{trans} is −1.0.

Normal values for kidney filtration and vascular parameters were calculated from our measurements, and compared with other (non-MRI) normal values from the literature (see Table 4). *Total kidney volume* was calculated from the pre-Gd T_1-weighted images for the 15 normal subjects. Values standardised to a body surface area (BSA) of 1.73 m^2 were also found; BSA was estimated from BSA(m²)=0.0235 height(cm)$^{0.422}$ weight(kg)$^{0.514}$ [28].

Results

Typical fits for the two phases of data are shown in Fig. 3. Sixty kidney image datasets were each fitted in two phases and with three VIRFs, giving a total of 360 fitting operations. The cubic interpolation of the aortic blood data gives a convincing description between the data points (Fig. 4) and enables timing parameters (Δ, T_g, T_{fwhm} , MRT) to be calculated with precision well below that of the imaging temporal resolution. Delayed exponential and Gaussian VIRFs fitted well. The onset of efflux from both the cortical and parenchymal regions could be detected (see for example Fig. 3a).

Comparing the three VIRFs in terms of the residuals from fits, for cortical and parenchymal regions in the perfusion phase, it was clear that the instant exponential VIRF performed significantly less well (RMS residual 4.3–6.5%) than the delayed exponential and Gaussian VIRFs (residuals 2.6–3.6%). Fractional blood volume v_b mean values and reproducibility (from the repeated examinations) were approximately the same for all VIRFs, for cortical and parenchymal ROIs and in both perfusion and uptake phases. The instant exponential VIRF was therefore excluded from subsequent analysis.

Comparing perfusion and uptake phases (for the estimation of v_b) showed that reproducibility was always slightly better using uptake phase data, for both cortical and parenchymal ROIs (although the residuals from the fits were slightly higher in the uptake phase). The hypothesis that the perfusion phase would estimate perfusion parameters better than the uptake phase, and justify the extra complexity of carrying out two fits, was therefore disproved, and perfusion phase data were not further analysed.

Measured normal values, residuals and measurement precision (ISD) are summarised in Tables 1 and 2.

Total filtration GFR values for increasingly large ROIs reached a plateau (Fig. 5). The datasets analysed showed similar behaviour, although some had a less obvious

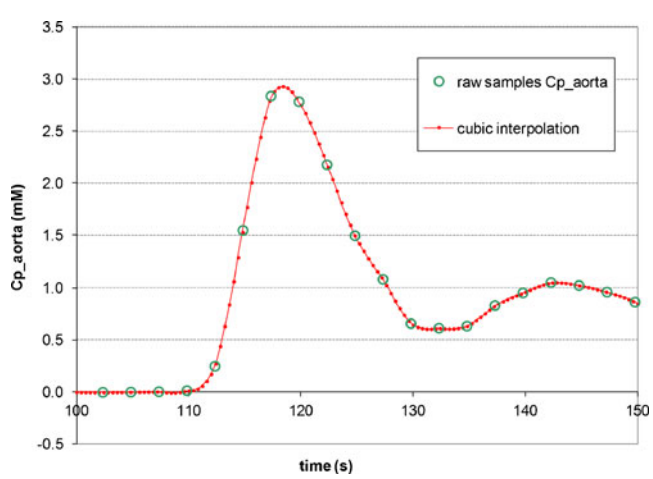

Fig. 4 Estimated arterial plasma concentration from blood signal, using cubic interpolation; note detail in peak not present in raw data

Table 2 Perfusion parameters from the uptake phase of repeated imaging of 15 healthy volunteers. Residuals are shown in Table 1 and symbols in Table 5

v_b (%)			*MRT* (s)			$F^{peak\ a}$			$F^{MRT\ a}$		
Mean	SD[b]	ISD[c]	Mean	SD	ISD	Mean	SD	ISD	Mean	SD	ISD
Cortical ROI, VIRF = delayed exponential											
41	10	7	5.20	0.66	0.35	542	150	104	482	127	77
Cortical ROI, VIRF = Gaussian											
40	10	8	4.68	0.68	0.37	310	80	44	523	138	71
Parenchymal ROI, VIRF = delayed exponential											
45	12	8	5.89	0.67	0.48	477	164	68	465	141	66
Parenchymal ROI, VIRF = Gaussian											
44	11	8	5.49	0.73	0.40	284	89	71	495	156	42

MRT = mean residence time

[a]From peak and MRT of delayed exponential or Gaussian VIRF; units: ml blood min^{-1} (100 ml tissue)$^{-1}$

[b]Group SD

[c]Instrumental SD (from repeated imaging)

plateau, with GFR_ROI increasing beyond the nominal parenchymal outline. The plateau value was 11.2± 2.8 ml min^{-1} (mean ± SD; 2 subjects, 8 kidneys). Typical values for a GFR_ROI calculation in a nominally cortical ROI were: K^{trans}=0.23 min^{-1}; ROI size=361 pixels; voxel volume 73 mm^3; GFR_ROI=6.1 ml min^{-1}. The effective number of slices per kidney was 5.8 (taking into account that peripheral slices contain smaller volumes of kidney); thus the parenchymal data give an estimate for total GFR of about 130 ml min^{-1} by this method, in agreement with other methods (see Table 4).

Sensitivity analysis is shown in Table 3. This confirms the large influence that the fixed parameters haematocrit, relaxivity, T_{10} and FA have on the estimated values of tissue parameters (principally filtration, blood volume and perfusion). Mean residence time is unaffected by fixed parameter errors, whilst the filtration fraction is more robust than filtration or perfusion. Small deviations in fixed parameters were used (~1–3%) to avoid non-linear effects, and the resulting EPR values had small random errors (~1%); thus a measured EPR of 0.99 could in fact be 1.00.

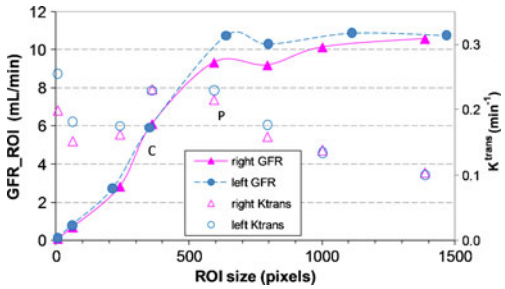

Fig. 5 In a central kidney slice, glomerular filtration rate (GFR) in progressively larger ROIs increases to a plateau value of about 11 ml min^{-1}; for five slices per kidney this gives a total GFR of 110 ml min^{-1} (single kidney GFR=55). Nominal cortical (C=350 pixels) and parenchymal (P=600 pixels) ROIs are shown. Mean K^{trans} values for small cortical ROIs vary, then decrease progressively for ROIs larger than the cortex

Normal values for kidney filtration and vascular parameters, measured using other (non-MRI) methods, were taken from the literature (see Table 4), and our measurements were compared with these. Kidney volume V_{kid} was estimated from a published value of mass m_{kid} as follows. The mass was measured post-mortem and therefore excludes most of the blood (which would drain out after removal). If a fraction of blood α remains in the parenchyma, then $V_{kid} = \frac{m_{kid}}{\rho(1-(1-\alpha)v_b)}$, where ρ is the kidney density. Using m_{kid}=150 g [29], ρ= 1.03 g ml^{-1}, α=10%, v_b=35% gives V_{kid} =213 ml, close to a published value of 218 ml [30].

The small vessel haematocrit value Hct^{small} is much lower than Hct^{large} (red blood cells have difficulty entering

Table 3 Sensitivity analysis showing how fitted (free) parameters (K^{trans} etc.) are affected by chosen value of fixed parameter (e.g. Hct^{large}). Values are error propagation ratio (EPR; i.e. percentage change in fitted parameter for 1% change in fixed parameter) [27]. Symbols are defined in Table 5

	$K^{trans\ b}$	$v_b{}^a$	F^b	*MRT*	*FF*
Fixed tissue parameters					
Hct^{large}	−0.72	−0.69	−0.70	0	0
Hct^{small}	0	+0.69	+0.69	0	0
$r_1{}^{blood}$	+0.98	+1.03	+1.03	0	0
$r_1{}^{d}$	−0.97	0	0	0	−0.99
$r_1{}^{iv}$	0	−0.98	−0.98	0	+0.99
$r_1{}^{iv}=r_1{}^{blood}$	+0.99 [c]	0	0	0	+0.99
$T_{10}{}^{blood}$	+1.04	+1.24	+1.29	0.02	−0.22
$T_{10}{}^{kidney}$	−1.06	−1.08	−1.14	0	+0.22
Fixed instrumental parameters					
θ	−0.07	+0.25	+0.29	0.03	−0.38
TR	0	−0.13	−0.15	0	+0.16

[a] Average from delayed exponential and Gaussian VIRFs

[b] Average of 4 F values from delayed exponential and Gaussian VIRFs, using both peak and MRT (see Eqs. 15, 16, 18, 19 in ESM)

[c] $r_1{}^{iv}$ fixed = $r_1{}^{blood}$; both altered together

Table 4 Comparison of normal parenchymal renal parameters estimated using DCE-MRI with published values. Thirty normal kidneys were each measured twice, using the uptake phase and Gaussian VIRF. Using a lower value for small-vessel haematocrit dramatically reduces values for blood volume (right-hand column)

		MRI Hct^{small}=41% Mean (SD)	Instrumental SD (CV)	Literature value	MRI Hct^{small}=24% Mean (SD)
Filtration (min^{-1})	K^{trans}	0.25 (0.05)	0.04 (18%)	0.28[a]	0.25 (0.05)
Mean residence time (s)	MRT	5.5 (0.7)	0.4 (7%)	6.5[b]	5.5 (0.7)
Blood volume (%)	v_b	44 (11)	8 (18%)	35[c]	34 (8)
Perfusion[d] ml blood min^{-1} (100 ml tissue)$^{-1}$	F	284 (89)	72 (14%)[e]	264[f]	219 (67)
Filtration fraction (%) [g]	FF	15.5 (2.9)	1.5 (9%)	15–20[h]	15.5 (2.9)
Absolute single kidney volume (ml)	V_{kid}	230 (28)	Not measured	213[i]	230 (28)
Standardised single kidney volume (ml) [j]	V_{kid}*	214 (20)	Not measured	213[i]	214 (20)
Total GFR (ml min^{-1})	GFR	115 (27) [k]	Not measured	125[h]	115 (27)[k]

CV Coefficient of Variation

[a] GFR/(2V_{kid}*)

[b] Measured using MRI by Sourbron [6]: 'plasma transit time TP'; SD=1.3 s

[c] From CT [43]

[d] From peak of Gaussian VIRF F_{gauss}^{peak}; average perfusion over parenchymal ROI; plasma perfusion is independent of Hct^{small} (see text)

[e] ISD of cortical perfusion is better (14%; see Table 2)

[f] Mean parenchymal perfusion = RBF/2*V_{kid}; RBF=1.1 l min [1, 46]

[g] Using Eq. 10

[h] Typical for young adult males [46]

[i] Estimated using mass=150 g (see text)

[j] I.e. corrected for body surface area (see text)

[k] 2 K^{trans} V_{kid}

small channels); values of 24% (dog heart) [31], 31% (human brain) [32], 25% [33] and 8–20% [34] have been reported. This is related to the Fahraeus effect; in small vessels red blood cells travel faster than plasma [34, 35]. The renal vasa recta (10–20 μm in diameter) have a reduced haematocrit of 40–50% compared with a large vessel [36]; the network Fahraeus effect can further reduce this by as much as 20% [34].

The MRI values were recalculated using a value of 24% for Hct^{small} (Table 4, right hand column); blood volume values then agreed with literature values. Left-sided cortical values of v_b and F were significantly higher than right-sided values ($P<10^{-8}$).

The effect on our normal values of altering the fixed tissue parameters revealed the following. Reducing T_{10}^{kid} from 1.2 s to 1.1 s (a plausible value for a parenchymal ROI dominated by cortical uptake; see Discussion in ESM) increased values of K^{trans}, v_b and F by about 9%, whilst leaving FF unaltered. Reducing r_1^d towards the low values indicated by rat studies [37] (e.g. 2.0 s^{-1} mM^{-1}; see Discussion in ESM) gave unrealistically high values of K^{trans} (0.56 min^{-1}), whilst leaving v_b, F and FF unaltered.

Discussion

A much fuller discussion is given in the Electronic Supplementary Material (ESM).

Imaging biomarkers and renal function

The kidney has many functions in maintaining homeostasis, one of which, glomerular filtration, is critical in both clinical nephrology and kidney research. The kidney's filtration fraction (FF) is defined as the ratio of GFR to renal plasma flow (RPF); however, RPF is difficult to measure (both experimentally and clinically). The mathematical model presented in this paper provides parameters that can give quantitative single kidney renal perfusion and GFR values as well as measurements of blood volume and FF (Table 4).

Existing MRI techniques

Various models [1–11] have been proposed for analysis of renal filtration using DCE-MRI. A critical review [38] showed that none of the published methods was sufficiently

accurate to be clinically accepted. The Patlak model and graphical analysis approach have been proposed for renal MRI [4, 17, 39–41], and comparisons have been made [1, 5] with more modern models.

Computed tomography

In DCE-CT imaging [41–43] the relationship between tracer concentration and signal intensity is linear. However partial volume effects and the estimation of small vessel haematocrit are problems for both CT and MRI.

Benefits of this model

Analysis of the early (uptake) phase of DCE-MRI using this model measures a few critical biomarkers of kidney function, namely vascular parameters and filtration. By restricting the time period over which the data are analysed (i.e. excluding efflux of tracer from the ROI), a simpler model can be used, designed specifically to measure vascular parameters and filtration. By analysing parenchymal (not cortical) ROIs, this analysis period has been extended to 90 s. This gives a time window where the domination of signal behaviour by filtration can be exploited using an optimal model, which is simple and therefore precise. Only a single free parameter is required to characterise renal function. The model represents the complexity of the actual kidney DCE-MRI signal data (Fig. 3) whilst avoiding undue further complexity; this probably contributes to being able to estimate the model parameters reliably [44]. This is an example of Occam's razor, which states that if a variety of explanations of a phenomenon are available, then in the absence of any other information, the simplest one is to be preferred.

Two additional kidney parameters are produced in this analysis. The filtration fraction (Eq. 10) is a valuable parameter in diabetes and other clinical diseases. The mean residence time (MRT) is very stable (Table 4), and its physiological significance needs to be evaluated. Although the MRT is measured from the aortic ROI, transit along the renal artery is rapid [45].

Shortcomings of DCE-MRI measurements

Uncertainty in the haematocrit value affects some of the tissue parameters and a realistic value for small vessel haematocrit (Hct^{small}) is required. The relationship between renal blood and plasma flow is not straightforwardly given by the large vessel haematocrit (as implied in text books [46]), and CT measurements would be equally affected. The higher values in the left-sided kidneys are probably an artefact, for which a possible explanation is poor slice profile [47].

Tissue parameter estimates are vulnerable to errors in haematocrit, tissue relaxivity, T_{10} and flip angle (Table 3). Estimates of renal plasma flow F_p (and also plasma volume v_p) are independent of Hct^{small}, and F_p might be a more useful tissue parameter than F. Our normal parenchymal values (from Table 4) are F_p=167 ml plasma min^{-1} (100 ml tissue)$^{-1}$, v_p=26%.

Relaxivity can alter in vivo from the in vitro values [37] and is probably the largest source of systematic error in DCE-MRI studies, as well as being unavoidable [48–50]. In disease, T_{10} is often raised, and should be measured explicitly if possible. In the absence of a measurement, then published values must be used [23, 51, 52]. Flip angle errors are likely at 3 T; a simple B_1 mapping technique [53] takes only a few minutes.

Cortical and parenchymal ROIs For estimation of filtration the entire parenchyma needs to be included in the ROI as the filtrate progresses relentlessly down the tubules into the medulla and back up to the cortex. Thus, the nominally cortical ROIs seriously underestimate uptake (Fig. 5). The

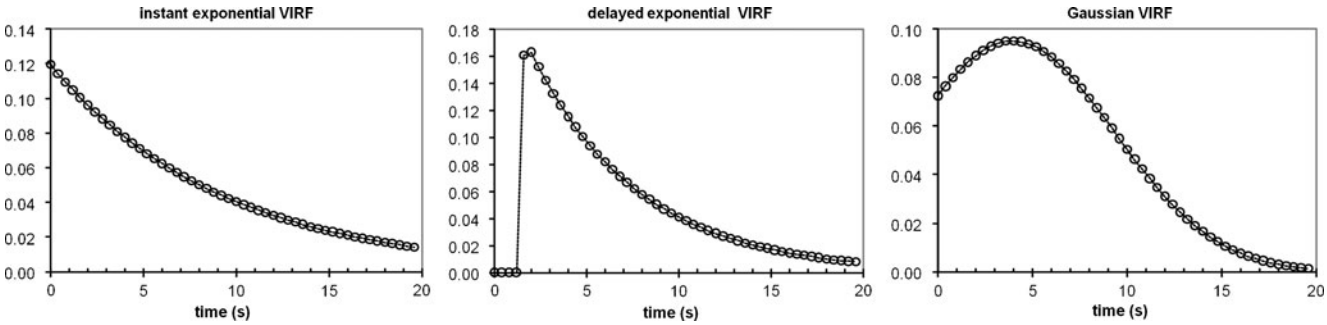

Fig. 6 Vascular impulse response functions (VIRFs). All fitted the data shown in Fig. 3a (parenchymal ROI, uptake phase) and have unit area. The instant exponential VIRF modelled the delayed perfusion peak badly. Differing peak values give rather different estimates for perfusion (see Table 2), although mean residence times are similar for both delayed VIRFs

Table 5 Parameters used for modelling

Quantity	Symbol	Units	Type
Concentration in aortic blood	C_b	mM	
Concentration in extravascular space	C_d	mM	
Concentration in aortic plasma	C_p^{aorta}	mM	
Concentration in kidney plasma	C_p^{kid}	mM	
Concentration in kidney tissue	C_t	mM	
VIRF delay	Δ	s	Free
Perfusion	F	ml blood (100 ml tissue)$^{-1}$ min^{-1}	
Filtration fraction	FF	%	
Flow into extravascular space per unit volume of tissue	F_1	mmol s^{-1} ml^{-1}	
Flow out of extravascular space per unit volume of tissue[a]	F_2	mmol s^{-1} ml^{-1}	
Flip angle	θ	Degrees	Fixed (17°)
Haematocrit in large vessels	Hct^{large}	%	Fixed (41%)
Haematocrit in capillaries	Hct^{small}	%	Fixed (41% or 24%)
Filtration (= GFR per unit volume of tissue)	K^{trans}	min^{-1} [b]	Free
Mean residence time[c]	MRT	s	
T_1 relaxivity in blood	r_1^{blood}	s^{-1} mM^{-1}	Fixed (4.5 s^{-1} mM^{-1}) [21]
T_1 relaxivity in extravascular space	r_1^{d}	s^{-1} mM^{-1}	Fixed (4.5 s^{-1} mM^{-1})
T_1 relaxivity in intravascular space	r_1^{iv}	s^{-1} mM^{-1}	Fixed (4.5 s^{-1} mM^{-1})
Pre-Gd blood signal	$S(0)^{blood}$	A.U.	Pre-calculated[d]
Pre-Gd tissue signal	$S(0)^{kidney}$	A.U.	Pre-calculated[d]
T_1 of blood	T_{10}^{blood}	s	Fixed (1.4 s)
T_1 of kidney	T_{10}^{kidney}	s	Fixed (1.2 s)
Gaussian VIRF width	T_{fwhm}	s	Free
Exponential VIRF width	T_g	s	Free
TR	TR	s	Fixed (1.6 ms)
Fractional blood volume in kidney	v_b	$0<v_b<1$	Free
Fractional plasma volume in kidney	v_p	$0<v_p<1$	

[a] Used for model with efflux (Eqs. 20, 21)

[b] Or can be expressed in ml min^{-1} (100 ml tissue)$^{-1}$ to be compatible with F

[c] From VIRF

[d] For each dataset, found from pre-Gd blood and tissue signals (arbitrary units)

variable ROI definition is probably a major contributor to within-subject variation [54].

VIRF shapes None of the VIRFs used in this work (see Fig. 6) is completely satisfactory; this is unsurprising given the complexity of renal anatomy, and the precise form is unimportant for estimation of filtration (and hence GFR) or blood volume (Table 1). An instant exponential model of the renal VIRF does not fit the vascular peak as well as a delayed exponential or Gaussian, although it has been used in the two-compartment exchange model (2CXM) [55]. The 2CXM may be too simple a model for kidney vasculature. Work is in progress to identify appropriate VIRFs.

The model has been extended to cover efflux, by adding a single extra free parameter [14] (see ESM).

Clinical studies will establish whether the DCE-MRI parameters will be sensitive to alterations in disease state such as focal renal damage in reflux nephropathy, disease states that affect the kidneys asymmetrically (obstruction or stone disease) or following renal transplantation. If these DCE-MRI biomarkers are shown to be reproducible then the clinician will have a non-invasive tool that avoids any radiation burden, and a quick single test will provide both anatomy and physiological parameters of each kidney separately. Recent publications show the advantage of quantitative renal perfusion measurements over conventional MRA [56, 57]. Our study has established the feasibility of using our model to measure both blood flow parameters and filtration with good reproducibility and reasonable accuracy in normal volunteers (Table 4).

Conclusion

Our model will calculate perfusion, filtration, filtration fraction, mean residence time, blood volume and single kidney GFR. It has been simplified by using uptake–phase time-domain data from parenchymal ROIs, it deals with signal non-linearity, it uses a reasonably realistic vascular impulse response function, and it recognises a reduced value of small vessel haematocrit. This model now needs to be evaluated on datasets from other centres, and in patients.

Acknowledgements Prof. David Buckley and Dr Steven Sourbron generously provided insightful and detailed comments and discussion. Dr Sheldon Cooper brought Occam's razor to our attention. Prof. Kenneth Miles contributed to the design of this project. Kidney Research UK sponsored acquisition of the volunteer data.

Appendix: Two-compartment mathematical model with broadening and delay of vascular peak

A1 Mathematical model (Fig. 1)

The perfusion peak (first pass of the bolus) in the kidney tissue data is consistently delayed and broadened compared with that in the arterial blood curve (see Fig. 2). Here the intravascular plasma concentration in the kidney $C_p^{kid}(t)$ is modelled as a convolution of the arterial plasma concentration $C_p^{art}(t)$ with a simple normalised vascular impulse response function (VIRF) *g(t)*:

$$C_p^{kid}(t) = C_p^{art}(t) \otimes g(t) = \int_0^t C_p^{art}(t-\tau) g(\tau) d\tau \tag{1}$$

$$\int_0^\infty g(t)dt = 1 \tag{2}$$

Thus *g(t)* is the IV response to an arterial delta function. Depletion of IV Gd by filtration is assumed to be small (i.e. $FF \ll 1$). The VIRF gives a variable delay and broadening. Several functions for *g(t)* were investigated (see below).

The rate of uptake F_1 into the renal extravascular space (filtration) is proportional to the IV concentration:

$$v_d \frac{dC_d(t)}{dt} = F_1 = K^{trans} C_p^{kid}(t) \tag{3}$$

v_d is the fractional volume of the renal EV space ($0<v_d<1$), $C_d(t)$ is the time-dependent concentration in this space, and F_1 is the flow rate of Gd into the EV compartment. K^{trans} here is the filtration (GFR) per unit volume of tissue; it is formally the unidirectional local transfer constant [12] for Gd from the IV space. The solution for $C_d(t)$ is a simple integral:

$$v_d C_d(t) = K^{trans} \int_0^t C_p^{kid}(\tau) d\tau \tag{4}$$

The concentration of IV tracer in tissue is $v_p C_p^{kid}$, where the fractional volume of the IV plasma space $v_p = v_b(1 - Hct^{small})$; v_b is the fractional blood volume in the kidney and Hct^{small} is the haematocrit in small vessels such as capillaries. The total Gd tissue concentration $C_t(t)$ is then the sum of the IV and EV contributions (which we have in Eqs. 1 and 4):

$$C_t(t) = v_b(1 - Hct^{small}) C_p^{kid} + v_d C_d(t) \tag{5}$$

The MRI signal enhancement from a given Gd concentration *C(t)* in blood or tissue is straightforward (assuming fast exchange for water, so that all the water in a voxel is relaxed by all the Gd). The reduction in T_1 is given by:

$$R_1(t) = R_{10} + r_1 C_t(t) \tag{6}$$

R_1 is the relaxation rate ($R_1=1/T_1$), R_{10} ($=1/T_{10}$) is its native (i.e. pre-Gd) value (before injection of contrast agent) and r_1 is the relaxivity (change in relaxation rate per unit concentration of Gd). The possibility of differing relaxivities in the IV space, the EV space and the arterial blood can be incorporated into fuller versions of this equation for tissue and blood:

$$\begin{aligned} R_1^{kidney}(t) &= R_{10}^{kidney} + r_1^{iv} v_b (1 - Hct^{small}) C_p^{kid}(t) + r_1^d v_d C_d(t) \\ R_1^{blood}(t) &= R_{10}^{blood} + r_1^{blood} C_b(t) \end{aligned} \tag{7}$$

where individual values r_1^{iv}, r_1^d, r_1^{blood} are used for each compartment (see Table 5).

The signal from a spoilt gradient echo sequence is:

$$S(t) = S_0 \frac{(1 - e^{-R_1(t)TR}) \sin\theta}{1 - e^{-R_1(t)TR} \cos\theta} \tag{8}$$

where θ is the flip angle.

The Gd concentration in the artery $C_p^{art}(t)$ (required for Eq. 1) is obtained from the measured blood signal as follows. Given $S(0)^{blood}$ (measured before the arrival of Gd) and T_{10}^{blood} we can find S_0^{blood} (from Eq. 8). From the observed blood signal (time–intensity curve) $S(t)^{blood}$ can then be found $R_1^{blood}(t)$ (Eq. 8). We can find the Gd concentration in arterial blood $C_b^{art}(t)$ (using Eq. 7). The concentration in plasma is then related by:

$$C_b{}^{art}(t) = (1 - Hct^{large}) C_p{}^{art}(t) \tag{9}$$

where Hct^{large} is the haematocrit in arteries.

The curve-fitting procedure, the discrete representation of the continuous functions at a temporal resolution of 0.4 s, spreadsheet implementation and interpolation of the AIF using Everett's formula for cubic interpolation [58] are all described in the ESM.

A2: Vascular impulse response functions: estimation of perfusion and filtration fraction

Three VIRFs were implemented as discrete functions (see ESM), forced to zero for t<0 and normalised to have a unit area over their finite duration (up to about 20 s), i.e. $\sum_i g_i(\tau)d\tau = 1$ (Fig. 6). For each, the mean residence time (MRT) was found from the first moment of *g(t)*.

Perfusion *F* was estimated from the VIRF peak or MRT. The filtration fraction is then simply the ratio of GFR to renal plasma flow $F(1\text{-}Hct^{small})$:

$$FF = \frac{K^{trans}}{(1 - Hct^{small})F} \tag{10}$$

References

1. Annet L, Hermoye L, Peeters F, Jamar F, Dehoux JP, Van Beers BE (2004) Glomerular filtration rate: assessment with dynamic contrast-enhanced MRI and a cortical-compartment model in the rabbit kidney. J Magn Reson Imaging 20:843–849
2. Pedersen M, Shi Y, Anderson P, Stodkilde-Jorgensen H, Djurhuus JC, Gordon I, Frokiaer J (2004) Quantitation of differential renal blood flow and renal function using dynamic contrast-enhanced MRI in rats. Magn Reson Med 51:510–517
3. Dujardin M, Sourbron S, Luypaert R, Verbeelen D, Stadnik T (2005) Quantification of renal perfusion and function on a voxel-by-voxel basis: a feasibility study. Magn Reson Med 54:841–849
4. Hackstein N, Kooijman H, Tomaselli S, Rau WS (2005) Glomerular filtration rate measured using the Patlak plot technique and contrast-enhanced dynamic MRI with different amounts of gadolinium-DTPA. J Magn Reson Imaging 22:406–414
5. Buckley DL, Shurrab AE, Cheung CM, Jones AP, Mamtora H, Kalra PA (2006) Measurement of single kidney function using dynamic contrast-enhanced MRI: comparison of two models in human subjects. J Magn Reson Imaging 24:1117–1123
6. Sourbron SP, Michaely HJ, Reiser MF, Schoenberg SO (2008) MRI-measurement of perfusion and glomerular filtration in the human kidney with a separable compartment model. Invest Radiol 43:40–48
7. Zhang JL, Rusinek H, Bokacheva L, Lerman LO, Chen Q, Prince C, Oesingmann N, Song T, Lee VS (2008) Functional assessment of the kidney from magnetic resonance and computed tomography renography: impulse retention approach to a multicompartment model. Magn Reson Med 59:278–288
8. Dujardin M, Luypaert R, Sourbron S, Verbeelen D, Stadnik T, de Mey J (2009) Age dependence of T1 perfusion MRI-based hemodynamic parameters in human kidneys. J Magn Reson Imaging 29:398–403
9. Bokacheva L, Rusinek H, Zhang JL, Lee VS (2008) Assessment of renal function with dynamic contrast-enhanced MR imaging. Magn Reson Imaging Clin N Am 16:597–611
10. Grenier N, Hauger O, Cimpean A, Perot V (2006) Update of renal imaging. Semin Nucl Med 36:3–15
11. Michaely HJ, Sourbron S, Dietrich O, Attenberger U, Reiser MF, Schoenberg SO (2007) Functional renal MR imaging: an overview. Abdom Imaging 32:758–771
12. Tofts PS, Brix G, Buckley DL, Evelhoch JL, Henderson E, Knopp MV, Larsson HB, Lee TY, Mayr NA, Parker GJ, Port RE, Taylor J, Weisskoff RM (1999) Estimating kinetic parameters from dynamic contrast-enhanced T(1)-weighted MRI of a diffusable tracer: standardized quantities and symbols. J Magn Reson Imaging 10:223–232
13. Leach MO, Brindle KM, Evelhoch JL, Griffiths JR, Horsman MR, Jackson A, Jayson GC, Judson IR, Knopp MV, Maxwell RJ, McIntyre D, Padhani AR, Price P, Rathbone R, Rustin GJ, Tofts PS, Tozer GM, Vennart W, Waterton JC, Williams SR, Workman P (2005) The assessment of antiangiogenic and antivascular therapies in early-stage clinical trials using magnetic resonance imaging: issues and recommendations. Br J Cancer 92:1599–1610
14. Tofts, PS, Mendichovszky IA, Buckley DL, Miles KA, Peters AM, Gordon I (2008) A simple two-compartment model that describes dynamic contrast-enhanced MRI signal in the kidney. Proc Intl Soc Mag Reson Med, 16th annual meeting, Toronto 454
15. Tofts, PS, Cutajar M, Mendichovszky IA, Gordon I (2009) Estimating GFR from early (uptake) portion of DCE MRI renal data, using a 3-compartment model, improves reproducibility and may eliminate need for cortical segmentation. Proc Intl Soc Mag Reson Med, 17th annual meeting, Honolulu 408
16. Tofts PS, Cutajar M, Mendichovszky IA, Gordon I (2010) Accurate and precise measurement of renal filtration and vascular parameters using DCE-MRI and a 3-compartment model. Proc Intl Soc Mag Reson Med, 18th annual meeting, Stockholm 326
17. Hackstein N, Heckrodt J, Rau WS (2003) Measurement of single-kidney glomerular filtration rate using a contrast-enhanced dynamic gradient-echo sequence and the Rutland-Patlak plot technique. J Magn Reson Imaging 18:714–725
18. de Senneville BD, Mendichovszky IA, Roujol S, Gordon I, Moonen C, Grenier N (2008) Improvement of MRI-functional measurement with automatic movement correction in native and transplanted kidneys. J Magn Reson Imaging 28:970–978
19. Peters AM, Brown J, Crossman D, Brady AJ, Hemingway AP, Roddie ME, Allison DJ (1990) Noninvasive measurement of renal blood flow with technetium-99 m-DTPA in the evaluation of patients with suspected renovascular hypertension. J Nucl Med 31:1980–1985
20. Boron WF, Boulpaep EL (2008) Medical physiology. Saunders, Philadelphia
21. Tofts PS, Shuter B, Pope JM (1993) Ni-DTPA doped agarose gel—a phantom material for Gd-DTPA enhancement measurements. Magn Reson Imaging 11:125–133
22. Spees WM, Yablonskiy DA, Oswood MC, Ackerman JJ (2001) Water proton MR properties of human blood at 1.5 Tesla: magnetic susceptibility, T(1), T(2), T*(2), and non-Lorentzian signal behavior. Magn Reson Med 45:533–542
23. de Bazelaire CM, Duhamel GD, Rofsky NM, Alsop DC (2004) MR imaging relaxation times of abdominal and pelvic tissues measured in vivo at 3.0 T: preliminary results. Radiology 230:652–659
24. Bland JM, Altman DG (1986) Statistical methods for assessing agreement between two methods of clinical measurement. Lancet 1:307–310
25. Tofts PS (2003) Quantitative MRI of the brain: measuring changes caused by disease. Wiley, New York
26. Tofts PS, Silver NC, Barker GJ, Gass A (2005) Object strength—an accurate measure for small objects that is insensitive to partial volume effects. MAGMA 18:162–169

27. Tofts PS, Berkowitz B, Schnall MD (1995) Quantitative analysis of dynamic Gd-DTPA enhancement in breast tumors using a permeability model. Magn Reson Med 33:564–568
28. Gehan EA, George SL (1970) Estimation of human body surface area from height and weight. Cancer Chemother Rep 54:225–235
29. Gray HG (1918) Anatomy of the human body
30. Tauxe WN, Todd-Pokropek A, Soussaline F, Raynaud C, Kellershohn C (1983) Estimates of kidney volume by single photon emission tomography: a preliminary report. Eur J Nucl Med 8:72–74
31. Crystal GJ, Downey HF, Bashour FA (1981) Small vessel and total coronary blood volume during intracoronary adenosine. Am J Physiol 241:H194–H201
32. Sakai F, Nakazawa K, Tazaki Y, Ishii K, Hino H, Igarashi H, Kanda T (1985) Regional cerebral blood volume and hematocrit measured in normal human volunteers by single-photon emission computed tomography. J Cereb Blood Flow Metab 5:207–213
33. Rempp KA, Brix G, Wenz F, Becker CR, Guckel F, Lorenz WJ (1994) Quantification of regional cerebral blood flow and volume with dynamic susceptibility contrast-enhanced MR imaging. Radiology 193:637–641
34. Pries AR, Ley K, Gaehtgens P (1986) Generalization of the Fahraeus principle for microvessel networks. Am J Physiol 251: H1324–H1332
35. Lamkin-Kennard KA, Jaron D, Buerk DG (2004) Impact of the Fahraeus effect on NO and O2 biotransport: a computer model. Microcirculation 11:337–349
36. Gaehtgens P (1980) Flow of blood through narrow capillaries: rheological mechanisms determining capillary hematocrit and apparent viscosity. Biorheology 17:183–189
37. Shuter B, Tofts PS, Wang SC, Pope JM (1996) The relaxivity of Gd-EOB-DTPA and Gd-DTPA in liver and kidney of the Wistar rat. Magn Reson Imaging 14:243–253
38. Mendichovszky I, Pedersen M, Frokiaer J, Dissing T, Grenier N, Anderson P, McHugh K, Yang Q, Gordon I (2008) How accurate is dynamic contrast-enhanced MRI in the assessment of renal glomerular filtration rate? A critical appraisal. J Magn Reson Imaging 27:925–931
39. Patlak CS, Blasberg RG, Fenstermacher JD (1983) Graphical evaluation of blood-to-brain transfer constants from multiple-time uptake data. J Cereb Blood Flow Metab 3:1–7
40. Prigent A, Cosgriff P, Gates GF, Granerus G, Fine EJ, Itoh K, Peters M, Piepsz A, Rehling M, Rutland M, Taylor A Jr (1999) Consensus report on quality control of quantitative measurements of renal function obtained from the renogram: International Consensus Committee from the Scientific Committee of Radionuclides in Nephrourology. Semin Nucl Med 29:146–159
41. Miles KA, Leggett DA, Bennett GA (1999) CT derived Patlak images of the human kidney. Br J Radiol 72:153–158
42. Helck A, Sommer WH, Klotz E, Wessely M, Sourbron SP, Nikolaou K, Clevert DA, Notohamiprodjo M, Illner WD, Reiser M, Becker HC (2010) Determination of glomerular filtration rate using dynamic CT-angiography: simultaneous acquisition of morphological and functional information. Invest Radiol 45:387–392
43. Tsushima Y, Blomley MJ, Kusano S, Endo K (1999) Use of contrast-enhanced computed tomography to measure clearance per unit renal volume: a novel measurement of renal function and fractional vascular volume. Am J Kidney Dis 33:754–760
44. Bokacheva L, Rusinek H, Zhang JL, Chen Q, Lee VS (2009) Estimates of glomerular filtration rate from MR renography and tracer kinetic models. J Magn Reson Imaging 29:371–382
45. Zubarev AV (2001) Ultrasound of renal vessels. Eur Radiol 11:1902–1915
46. Eaton DC, Pooler JP (2009) Vander's renal physiology. McGraw-Hill, New York
47. Gutierrez DR, Wells K, Diaz MO, Moran SA, Mendichovszky IA, Gordon I (2010) Partial volume effects in dynamic contrast magnetic resonance renal studies. Eur J Radiol 75:221–229
48. Rohrer M, Bauer H, Mintorovitch J, Requardt M, Weinmann HJ (2005) Comparison of magnetic properties of MRI contrast media solutions at different magnetic field strengths. Invest Radiol 40:715–724
49. Pedersen M, Vajda Z, Stodkilde-Jorgensen H, Nielsen S, Frokiaer J (2007) Furosemide increases water content in renal tissue. Am J Physiol Renal Physiol 292:F1645–F1651
50. Stanisz GJ, Henkelman RM (2000) Gd-DTPA relaxivity depends on macromolecular content. Magn Reson Med 44:665–667
51. Bluml S, Schad LR, Stepanow B, Lorenz WJ (1993) Spin-lattice relaxation time measurement by means of a TurboFLASH technique. Magn Reson Med 30:289–295
52. Jones RA, Ries M, Moonen CT, Grenier N (2002) Imaging the changes in renal T1 induced by the inhalation of pure oxygen: a feasibility study. Magn Reson Med 47:728–735
53. Dowell NG, Tofts PS (2007) Fast, accurate, and precise mapping of the RF field in vivo using the 180 degrees signal null. Magn Reson Med 58:622–630
54. Cutajar M, Mendichovszky IA, Tofts PS, Gordon I (2010) The importance of AIF ROI selection in DCE-MRI renography: reproducibility and variability of renal perfusion and filtration. Eur J Radiol 74:e154–e160
55. Donaldson SB, West CM, Davidson SE, Carrington BM, Hutchison G, Jones AP, Sourbron SP, Buckley DL (2010) A comparison of tracer kinetic models for T1-weighted dynamic contrast-enhanced MRI: application in carcinoma of the cervix. Magn Reson Med 63:691–700
56. Dujardin M, Luypaert R, Vandenbroucke F, Van der Niepen P, Sourbron S, Verbeelen D, Stadnik T, de Mey J (2009) Combined T1-based perfusion MRI and MR angiography in kidney: first experience in normals and pathology. Eur J Radiol 69:542–549
57. Attenberger UI, Sourbron SP, Schoenberg SO, Morelli J, Leiner T, Schoeppler GM, Samtleben W, Birkemeier KL, Glaser C, Reiser MF, Michaely HJ (2010) Comprehensive MR evaluation of renal disease: added clinical value of quantified renal perfusion values over single MR angiography. J Magn Reson Imaging 31:125–133
58. Scheid F (1968) Schaum's outline of theory and problems of numerical analysis. McGraw-Hill, New York